doi:10.1038/nature13391

Possible control of subduction zone slow-earthquake periodicity by silica enrichment

Pascal Audet[1] & Roland Bürgmann[2]

Seismic and geodetic observations in subduction zone forearcs indicate that slow earthquakes, including episodic tremor and slip, recur at intervals of less than six months to more than two years[1,2]. In Cascadia, slow slip is segmented along strike[3] and tremor data show a gradation from large, infrequent slip episodes to small, frequent slip events with increasing depth of the plate interface[4]. Observations[5–7] and models[8,9] of slow slip and tremor require the presence of near-lithostatic pore-fluid pressures in slow-earthquake source regions; however, direct evidence of factors controlling the variability in recurrence times is elusive. Here we compile seismic data from subduction zone forearcs exhibiting recurring slow earthquakes and show that the average ratio of compressional (P)-wave velocity to shear (S)-wave velocity (v_P/v_S) of the overlying forearc crust ranges between 1.6 and 2.0 and is linearly related to the average recurrence time of slow earthquakes. In northern Cascadia, forearc v_P/v_S values decrease with increasing depth of the plate interface and with decreasing tremor-episode recurrence intervals. Low v_P/v_S values require a large addition of quartz in a mostly mafic forearc environment[10,11]. We propose that silica enrichment varying from 5 per cent to 15 per cent by volume from slab-derived fluids and upward mineralization in quartz veins[12] can explain the range of observed v_P/v_S values as well as the downdip decrease in v_P/v_S. The solubility of silica depends on temperature[13], and deposition prevails near the base of the forearc crust[11]. We further propose that the strong temperature dependence of healing and permeability reduction in silica-rich fault gouge via dissolution–precipitation creep[14] can explain the reduction in tremor recurrence time with progressive silica enrichment. Lower gouge permeability at higher temperatures leads to faster fluid overpressure development and low effective fault-normal stress, and therefore shorter recurrence times. Our results also agree with numerical models of slip stabilization under fault zone dilatancy strengthening[15] caused by decreasing fluid pressure as pore space increases. This implies that temperature-dependent silica deposition, permeability reduction and fluid overpressure development control dilatancy and slow-earthquake behaviour.

Slow earthquakes—comprising slow fault slip, often accompanied by low-frequency tremor (also called episodic tremor and slip, or ETS)—generally recur at regular intervals on the plate interface within the forearc of young and warm subduction zones, downdip of the locked zone[1,2]. Their association with a dipping layer of extremely low seismic S-wave velocity, interpreted to represent near-lithostatic pore-fluid pressure within subducting oceanic crust, has been established in most locations[5–7], thus suggesting a link between fault zone hydrology and the fault–slip behaviour. Factors controlling ETS periodicity are poorly constrained. One possibility involves modulation by periodic external forces including seasonal hydrologic loads and the Earth's 14-month pole tides[16–18], but these cannot explain the wide range of observed periods. Segmentation of ETS behaviour in Cascadia correlates qualitatively with the overriding forearc structure and geology[3]; however, the exact nature of this relation is elusive. In northern Cascadia, tremor observations indicate a systematic decrease in the recurrence time of slow-slip events with increasing depth of the plate interface[4]. Wech and Creager's[4] conceptual interpretation of this observation involves a decrease in friction with increasing temperature, resulting in a weaker fault that ruptures more frequently at greater depths.

We compile observations of converted teleseismic waves (or receiver functions) from permanent and temporary broadband stations located in the forearc of circum-Pacific subduction zones where slow earthquakes (slow-slip with or without tremor) are known to occur at regular intervals, including Japan, Cascadia, Mexico, Costa Rica, and New Zealand (Fig. 1a, Extended Data Table 1). At each subduction zone we select stations closest to the inferred slow-earthquake source regions (Extended Data Fig. 1). In Cascadia we consider stations closer to the longer-recurrence ETS events at shallower depths[4,19]. These data are sensitive to structures with scale lengths of 1–10 km and are dominated by the signature of a dipping, low-velocity layer[6,19]. The low-velocity zones associated with the slow-earthquake slip areas have very high v_P/v_S values of 2.6 ± 0.3 (1σ), which have no apparent relationship with the slow-slip recurrence intervals (Fig. 1b). On the other hand, we see a linear and positive relation between the v_P/v_S of the overriding forearc crust and recurrence times of slow earthquakes (Fig. 1c). The forearc v_P/v_S results are in agreement with a number of studies that estimate forearc crust v_P/v_S using different forms of travel time tomography (Fig. 1c; see Methods), which generally show somewhat lower v_P/v_S owing to various forms of data regularization and smoothing.

Following previous studies, we interpret the high v_P/v_S values of the low-velocity layer to represent high, near-lithostatic pore-fluid pressure within subducting upper oceanic crust[6,7]. Elevated pore-fluid pressures imply that the plate interface represents a low-permeability boundary, presumably caused by mineral precipitation or grain size reduction. The ubiquity of overpressured oceanic crust in slow-earthquake source regions of warm subduction zones suggests that low effective stress on the megathrust is a necessary condition for the occurrence of slow earthquakes. The observed scatter in the low-velocity-zone v_P/v_S values and the absence of a relationship between v_P/v_S and recurrence times may indicate that the measured v_P/v_S values are only a snapshot of more dynamic and possibly fast-changing fluid processes within the oceanic crust. Exploring temporal variations in v_P/v_S may capture such processes, should these be resolvable. The seismic velocities of the overlying forearc crust seem to provide better constraints on the time-integrated effects of fluid flow and accumulation and the associated transport and precipitation of silica[11], which apparently correlate with the slow-slip behaviour.

The linear relationship between forearc crust v_P/v_S and the recurrence times of slow earthquakes (Fig. 1c) supports the hypothesis that the structure of the hanging wall of subduction zone forearcs reflects conditions that determine ETS behaviour[3,20]. We further examine this question by compiling seismic observations of hanging-wall v_P/v_S along a margin-perpendicular profile in northern Cascadia from published data[21]. Values of v_P/v_S progressively decrease from initially high (>1.85) to low (~ 1.65) values with increasing depth (from 20 km to 45 km) to the plate interface, indicating that progressively more overlying crust material with low bulk v_P/v_S is sampled (Fig. 2). Laboratory measurements of v_P/v_S for most crustal rocks at dry conditions fall in the range

[1]Department of Earth Sciences, University of Ottawa, Ottawa, Ontario K1N 6N5, Canada. [2]Department of Earth and Planetary Science and Berkeley Seismological Laboratory, University of California, Berkeley, California 94720-4767, USA.

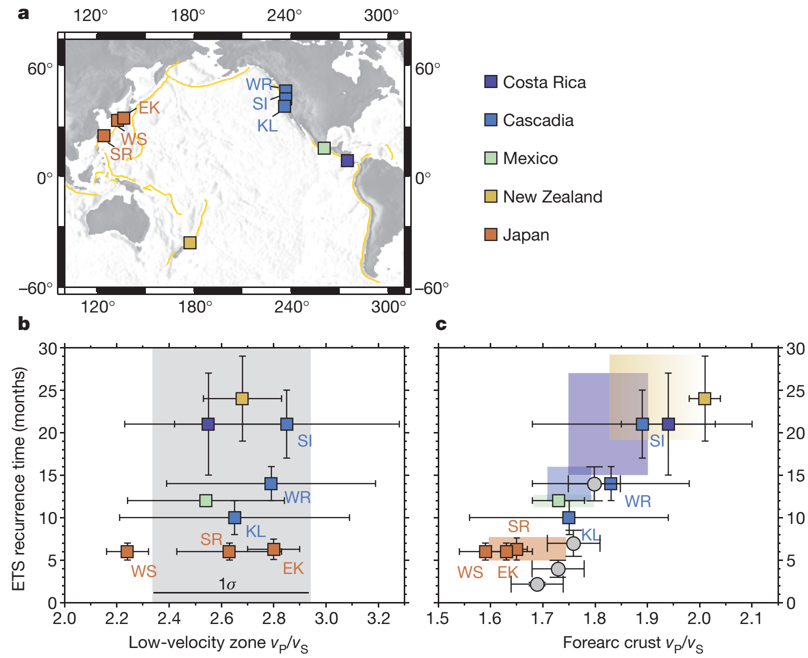

Figure 1 | Subduction zone velocity structure in slow-earthquake source regions. Recurrence times of slow earthquakes (selected regions shown in **a**; see Methods and Extended Data Table 2 for data sources) compared with v_P/v_S values of a dipping, low-velocity zone interpreted as subducting oceanic crust (**b**) and overriding forearc crust (**c**) (Extended Data Table 1 and Fig. 1). Error bars show 1σ uncertainty. High v_P/v_S values of subducting oceanic crust show a large scatter (1σ zone shown in grey) and are uncorrelated with recurrence times. In **c** the coefficient of correlation is 0.9 and a two-tailed Student's *t*-test shows a statistically significant correlation at the 95% level. Also shown in shaded colours are ranges of v_P/v_S estimates from various seismic tomography studies (Extended Data Table 2). Grey circles show along-dip variations in forearc v_P/v_S values[21] and tremor periodicity for northern Cascadia[4] (Fig. 2). Labels are SI, Siletzia; WR, Wrangellia; KL, Klamath; SR, Southern Ryukyu; WS, Western Shikoku; and EK, Eastern Kii peninsula.

of 1.7 to 1.85, with higher values found for more mafic compositions[10]. These ratios increase further at wet and slightly overpressured conditions[22], and the highest v_P/v_S values observed in the updip portion of the Cascadia profile may be explained by the presence of hydrated mafic lithologies and low-grade metamorphic facies. The lowest values require increasing proportions of silica-rich minerals and, in particular, quartz[23], characterized by the lowest velocity ratios ($v_P/v_S = 1.50 \pm 0.03$) determined in the laboratory at ambient temperatures[10,22], which decrease further with increasing temperatures up to the α-to-β phase transition (at >600 °C) of quartz[24].

Quartz-rich rocks are not typically found at those depths in the lower continental crust. Quartz enrichment may be caused by the precipitation of fluid-dissolved silica derived from the progressive dehydration of the downgoing slab. This scenario is supported by seismic[11], laboratory[13] and field evidence[12] that suggest quartz deposition to be progressively more important downdip owing to the temperature dependence of silica solubility in slab-derived fluids[13]. Our data support a massive addition of silica to the deep continental forearc crust, which may locally reach 20% quartz by volume[11]. Fossil examples of abnormally high concentration of quartz veins include giant mesothermal gold deposits that formed during greenschist facies metamorphism in accretionary complexes[25]. Although the estimated fluid flux required is about two orders of magnitude greater than fluid production rates estimated from slab dehydration processes in Cascadia[22] (see Methods), the availability of silica-saturated fluids from the slab may be greatly enhanced by complete serpentinization of the mantle near the wedge corner[26]. Silica enrichment as a function of subduction zone age, temperature and plate interface depth can explain the observed pattern of v_P/v_S variations within the overlying crust.

What causes the observed strong correlation between silica enrichment indicated by the forearc v_P/v_S data and decreasing slow-earthquake recurrence times? We postulate that abundant silica-rich fluids from the slab and increased temperatures accelerate the rate of permeability reduction in the fault zone, which plays a fundamental part in controlling fault strength and stability. At the pressure and temperature

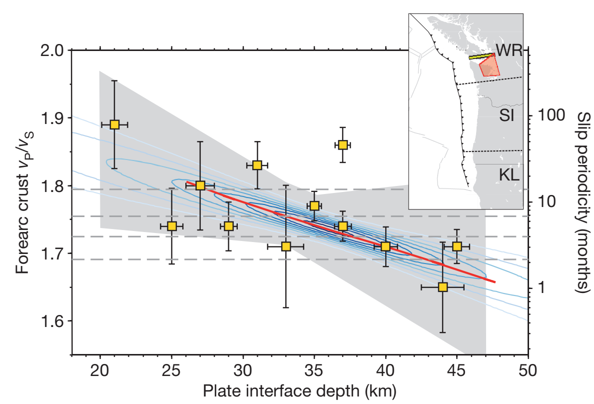

Figure 2 | Downdip v_P/v_S variations of overlying forearc crust in northern Cascadia. Seismic data (yellow squares; error bars show 1σ uncertainty) are from ref. 21. The linear trend of v_P/v_S as a function of plate interface depth[21] is used to match the position of the logarithmic decay (solid red line) of slip periodicity along dip[4]. The blue contours show the probability density function at constant intervals (0.01) for the range of linear regressions obtained from bootstrap analysis of the trend, with dark blue being more probable than pale blue. The shaded grey region outlines the range of linear regressions from the bootstrapped samples (see Methods). Horizontal dashed grey lines show v_P/v_S and slip periodicity values extracted at data points that were used to fit the exponential trend of tremor periodicity[4], plotted in Fig. 1. The inset shows the location of the v_P/v_S profile[21] (yellow box) and the area used for inferring decay of tremor periodicity[4] (red shaded area).

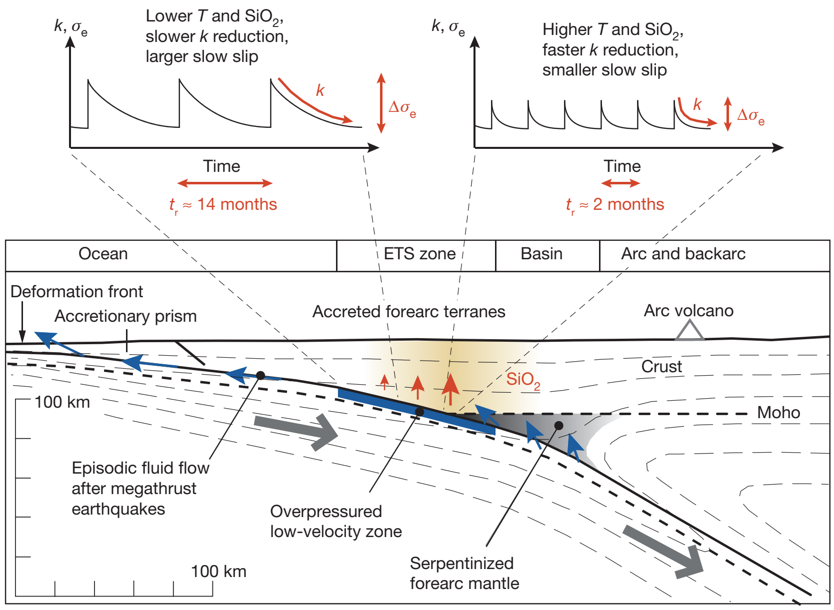

Figure 3 | Conceptual model of silica enrichment controlling slow-earthquake behaviour in northern Cascadia. Progressive silica deposition into quartz minerals and veins due to higher silica solubility with increasing temperature T at depth enriches the overlying forearc crust and decreases v_P/v_S values. Following a slow-slip event, permeability k increases, allowing fluid circulation and a reduction in pore-fluid pressure. Strong temperature-dependence of permeability reduction in quartz gouge leads to faster re-sealing, overpressure development (shown here as decreasing effective normal stress, σ_e) and thus lower recurrence times t_r with increasing temperature. Thin dashed lines are 200 °C isotherms. Moho, Mohorovičić discontinuity. This figure is modified from ref. 22, with permission.

conditions corresponding to tremor depths, rapid dissolution–precipitation creep processes in a semi-ductile shear zone control permeability reduction in quartz gouge[14]. Slow fault slip produces transient permeability increases in fault gouge, followed by resealing[14,27,28]. Faster healing and reduction in permeability may lead to faster recharge and overpressure development, and thus more rapid reduction in the effective fault-normal stress and more frequent slip events (Fig. 3). Assuming a constant stressing rate along dip, the apparent decrease in slip size with depth depends on stress drop[9]. Our model therefore suggests that stress drop is smaller when permeability reduction and pore-fluid pressure buildup increase more rapidly between slow-slip events. Our model is also consistent with the downdip initiation and updip migration of both large and small slow-slip events[4], where the updip segment of the plate interface does not always react to a downdip slip pulse because it remains stable at those timescales (that is, fluid overpressure and effective stress have not yet reached the critical threshold for slip). However, it is likely that slip pulses initiating downdip may bring the system to instability when updip conditions are close to critical.

This model can explain the relation between silica enrichment in the forearc crust and slow-earthquake recurrence time as a function of plate interface depth in northern Cascadia (Fig. 3). The control of silica gouge on recurrence time may also be applicable to the global (Fig. 1c) and regional[3] observations, if the absolute amount of silica enrichment is a proxy for conditions (temperature, fluids and fault zone mineralogy) that govern creep processes and healing rate in the fault zone. In Cascadia, ETS recurrence-time segmentation correlates with the geology of the forearc crust, where the younger, more mafic (silica-poor) Siletzia terrane has the highest v_P/v_S ratios and longest recurrence times compared with the older, more felsic (silica-rich) forearc terranes to the north and south with shorter recurrence times[3]. These observations are qualitatively consistent with a control of ETS behaviour by time-integrated and temperature-dependent silica enrichment of the forearc crust.

Numerical simulations of megathrust fault slip suggest that dilatancy strengthening plays an important role in controlling slow-slip behaviour[9,15]. In areas of strong dilatancy, pore opening is faster than pore-fluid diffusion during shear, which stabilizes slip and prevents the development of a seismic rupture. In these simulations, dilatancy also modulates the periodicity of slow-slip events, with increasing dilatancy leading to an increase of recurrence time, slip amplitude and duration of slow-slip events[15]. These models suggest that an updip increase of dilatancy in the slow-slip zone produces less frequent, slower-slipping ETS in the updip part and more frequent, faster-slipping short-term slip events at greater depths. However, it is not clear through which process changes in forearc v_P/v_S would produce, or be the result of, corresponding changes in dilatancy that lead to the observed linear relation with recurrence time. We speculate that temperature-dependent silica deposition, permeability reduction and overpressure development control dilatancy and thus slow-earthquake behaviour. The lower edge of the episodic slip zone presumably marks a transition to fully ductile flow controlled by dislocation creep, in which fluids act as a weakening factor but pore pressure and dilatancy effects are no longer important.

METHODS SUMMARY

Data used in this study come from several broadband seismic stations located in subduction zone forearcs that exhibit ETS (Extended Data Fig. 1). At each station we compile three-component data with high signal-to-noise ratio (>7.5 dB) on the vertical component from 1990–2011, surface-wave magnitude $M > 5.8$ earthquakes. Seismograms are decomposed into upgoing P- and S-wave modes and are deconvolved using Wiener spectral deconvolution. Receiver functions are filtered at corner frequencies of 0.05 Hz to 0.5 Hz and stacked into 7.5° back-azimuth and 0.002 s km^{-1} slowness bins. We model waveforms using a fast ray-based forward algorithm[29]. We use a two-layer crustal model with fixed P-wave velocity of 6.5 km s^{-1} composed of continental forearc crust overlying a dipping low-velocity layer representing subducting oceanic crust, underlain by a mantle half-space with fixed P- and S-wave velocities of 8.0 km s^{-1} and 4.5 km s^{-1}, respectively. Strike and dip of the low-velocity layer are taken from global and local slab models[30]. The misfit is calculated using a normalized correlation scheme and includes both radial and transverse components. Cumulative variance within each receiver function bin is used as an inverse weight in the misfit calculation and the Monte Carlo inversion for model parameters is carried out using a Neighbourhood Algorithm[31]. Results for Cascadia are taken directly from refs 19 and 21. In Costa Rica we extract a subset of data from the southeastern Nicoya peninsula[20]. Extended Data Table 1 shows all other measurements for Japan, Mexico and northern New Zealand.

Online Content Any additional Methods, Extended Data display items and Source Data are available in the online version of the paper; references unique to these sections appear only in the online paper.

Received 3 December 2013; accepted 8 April 2014.

1. Schwartz, S. Y. & Rokosky, J. M. Slow slip events and seismic tremor at circum-Pacific subduction zones. *Rev. Geophys.* **45,** RG3004 (2007).
2. Beroza, G. C. & Ide, S. Slow earthquakes and nonvolcanic tremor. *Annu. Rev. Earth Planet. Sci.* **39,** 271–296 (2011).
3. Brudzinski, M. R. & Allen, R. M. Segmentation in episodic tremor and slip all along Cascadia. *Geology* **35,** 907–910 (2007).
4. Wech, A. G. & Creager, K. C. A continuum of stress, strength and slip in the Cascadia subduction zone. *Nature Geosci.* **4,** 624–628 (2011).
5. Shelly, D. R., Beroza, G. C., Ide, S. & Nakamula, S. Low-frequency earthquakes in Shikoku, Japan, and their relationship to episodic tremor and slip. *Nature* **442,** 188–191 (2006).
6. Audet, P., Bostock, M. G., Christensen, N. I. & Peacock, S. M. Seismic evidence for overpressured subducting oceanic crust and megathrust fault sealing. *Nature* **457,** 76–78 (2009).
7. Song, T.-R. A. *et al.* Subducting slab ultra-slow velocity layer coincident with silent earthquakes in southern Mexico. *Science* **324,** 502–506 (2009).
8. Liu, Y. & Rice, J. R. Spontaneous and triggered aseismic deformation transients in a subduction fault model. *J. Geophys. Res.* **112,** B09404 (2007).
9. Segall, P., Rubin, A. M., Bradley, A. M. & Rice, J. R. Dilatant strengthening as a mechanism for slow slip events. *J. Geophys. Res.* **115,** B12305 (2010).
10. Christensen, N. I. Poisson's ratio and crustal seismology. *J. Geophys. Res.* **101,** 3139–3156 (1996).
11. Ramachandran, K. & Hyndman, R. D. The fate of fluids released from subducting slab in northern Cascadia. *Solid Earth* **3,** 121–129 (2012).
12. Breeding, C. M. & Ague, J. J. Slab-derived fluids and quartz-vein formation in an accretionary prism, Otago Schist, New Zealand. *Geology* **30,** 499–502 (2002).
13. Manning, C. E. The solubility of quartz in H_2O in the lower crust and upper mantle. *Geochim. Cosmochim. Acta* **58,** 4831–4839 (1994).
14. Giger, S. B., Tenthorey, E., Cox, S. F. & Fitz Gerald, J. D. Permeability evolution in quartz gouges under hydrothermal conditions. *J. Geophys. Res.* **112,** B07202 (2007).
15. Liu, Y. Numerical simulations on megathrust rupture stabilization under strong dilatancy strengthening in slow slip region. *Geophys. Res. Lett.* **40,** 1311–1316 (2013).
16. Shen, Z.-K. *et al.* Pole-tide modulation of slow slip events at circum-Pacific subduction zones. *Bull. Seismol. Soc. Am.* **95,** 2009–2015 (2005).
17. Lowry, A. R. Resonant slow fault slip in subduction zones forced by climatic load stress. *Nature* **442,** 802–805 (2006).
18. Pollitz, F. F., Wech, A. G., Kao, H. & Bürgmann, R. Annual modulation of non-volcanic tremor in northern Cascadia. *J. Geophys. Res.* **118,** 2445–2459 (2013).
19. Hansen, R. T. J., Bostock, M. G. & Christensen, N. I. Nature of the low velocity zone in Cascadia from receiver function waveform inversion. *Earth Planet. Sci. Lett.* **337–388,** 25–38 (2012).
20. Audet, P. & Schwartz, S. Y. Hydrologic control of forearc strength and seismicity in the Costa Rican subduction zone. *Nature Geosci.* **6,** 852–855 (2013).
21. Audet, P. *et al.* Slab morphology in the Cascadia fore arc and its relation to episodic tremor and slip. *J. Geophys. Res.* **115,** B00A16 (2010).
22. Peacock, S. M., Christensen, N. I., Bostock, M. G. & Audet, P. High pore pressures and porosity at 35 km depth in the Cascadia subduction zone. *Geology* **39,** 471–474 (2011).
23. Lowry, A. R. & Pérez-Gussinyé, M. The role of crustal quartz in controlling Cordilleran deformation. *Nature* **471,** 353–357 (2011).
24. Kern, H. Elastic-wave velocity in crustal and mantle rocks at high pressure and temperature: the role of the high-low quartz transition and of dehydration reactions. *Phys. Earth Planet. Inter.* **29,** 12–23 (1982).
25. Sillitoe, R. H. Major gold deposits and belts of the North and South American Cordillera: distribution, tectonomagmatic settings, and metallogenic considerations. *Econ. Geol.* **103,** 663–687 (2008).
26. Wada, I. Wang. K., He, J. & Hyndman, R. D. Weakening of the subduction interface and its effects on surface heat flow, slab dehydration, and mantle wedge serpentinization. *J. Geophys. Res.* **113,** B04402 (2008).
27. Dempsey, D. E., Rowland, J. V., Zyvoloski, G. A. & Archer, R. A. Modeling the effects of silica deposition and fault rupture on natural geothermal systems. *J. Geophys. Res.* **117,** B05207 (2012).
28. Fisher, D. M. & Brantley, S. L. The role of silica redistribution in the evolution of slip instabilities along subduction interfaces: constraints from the Kodiak accretionary complex, Alaska. *J. Struct. Geol.* doi:10.1016/j.jsg.2014.03.010 (in the press).
29. Frederiksen, A. W. & Bostock, M. G. Modelling teleseismic waves in dipping, anisotropic structures. *Geophys. J. Int.* **141,** 401–412 (2000).
30. Hayes, G. P., Wald, D. J. & Johnson, R. L. Slab1.0: a three-dimensional model of global subduction zone geometries. *J. Geophys. Res.* **117,** B01302 (2012).

Acknowledgements Data used in this study come from the Japan Meteorological Agency, New Zealand National Seismograph Network, and the Tectonic Observatory (Caltech). Funding for this work comes from the Natural Science and Engineering Research Council (Canada) and the Miller Institute for Basic Research in Science (University of California, Berkeley). We thank N. Beeler, A. Rubin and P. Ampuero for discussions and comments.

Author Contributions P.A. performed data processing and inversion. Both P.A. and R.B. contributed to the interpretations and preparation of the final manuscript.

Author Information Reprints and permissions information is available at www.nature.com/reprints. The authors declare no competing financial interests. Readers are welcome to comment on the online version of the paper. Correspondence and requests for materials should be addressed to P.A. (pascal.audet@uottawa.ca).

METHODS

Receiver function analysis. Data used in this study come from several permanent and portable networks of broadband seismic stations located in the forearc of subduction zones that exhibit ETS (Extended Data Fig. 1). At each station we compile all available three-component data with high signal-to-noise ratio (>7.5 dB) on the vertical component from 1990–2011, magnitude $M > 5.8$ earthquakes at teleseismic distances. Seismograms are decomposed into upgoing P- and S-wave modes and are deconvolved using Wiener spectral deconvolution to obtain radial and transverse P-wave receiver functions. Receiver functions are then filtered at corner frequencies of 0.05 Hz to 0.5 Hz and stacked into 7.5° back-azimuth and 0.002 s km^{-1} slowness bins. Coherent signals on the receiver functions represent direct P-to-S conversions and free-surface P-to-S and S-to-S reverberations from velocity contrasts within the underlying column[21]. Each scattered phase displays oppositely polarized pulses that are characteristic of a prominent, dipping low-velocity layer.

Waveform modelling. We model waveforms using a fast ray-based forward algorithm for waves in dipping, anisotropic media[29]. We use a two-layer crustal model with fixed P-wave velocity of 6.5 km s^{-1} composed of continental forearc crust overlying a dipping low-velocity layer representing subducting oceanic crust, underlain by a mantle half-space with fixed P-wave and S-wave velocities of 8.0 km s^{-1} and 4.5 km s^{-1}, respectively. Parameters that we estimate are the thickness and v_P/v_S of each crustal layer. Our results are only weakly sensitive to variations in the background P-wave velocity structure. Strike and dip of the low-velocity layer are taken from global and local slab models[30]. The misfit is calculated using a normalized correlation scheme and includes both radial and transverse components. Cumulative variance within each receiver function bin is used as an inverse weight in the misfit calculation and the Monte Carlo inversion for model parameters is carried out using a Neighbourhood Algorithm[31]. Results for Cascadia are taken directly from refs 19 and 21. In Costa Rica we extract a subset of data from the southeastern Nicoya peninsula, where large slow slip occurs[20]. Extended Data Table 1 shows all other measurements for Japan, Mexico and northern New Zealand.

Fluid flux from quartz deposition. Our data suggest a massive addition of silica to the deep continental forearc crust, possibly reaching 20% quartz by volume locally[11]. Considering the time-integrated flux of 4.5×10^6 m^3 of fluids per m^2 of rock needed to precipitate quartz by regionally flowing fluids from an average local-equilibrium silica-solubility gradient at 350 °C–450 °C and 6–8 kbar (ref. 12), a 20% silica enrichment requires a steady-state fluid flux of about 20 mm yr^{-1} over the 40 million years of Cascadia subduction[11]. This flux is about two orders of magnitude higher than fluid production rates estimated from slab dehydration processes[22]. However, the local fluid production at the base of the crust near the mantle wedge corner may be greatly increased because complete retrograde serpentinization occurs early owing to the small wedge volume[24]. Silica-rich fluids are thus no longer consumed by further serpentinization, which may significantly increase fluid fluxes near the bottom of the forearc crust.

Bootstrap analysis. We performed a bootstrap analysis of the trend between forearc v_P/v_S and plate interface depth. For this analysis we extracted 10,000 random sets of samples (with replacement) from the original data and calculated both the coefficient of correlation ρ and the coefficient of determination r^2 from a linear regression of each set. Median values are 0.8 and 0.6 for ρ and r^2, respectively, indicating a reasonably good fit. Finally, we determined the probability density function of the bootstrapped regression lines as a function of plate interface depth. The result is a two-dimensional map of the probability density function based on the data, shown in Fig. 2 as contours of constant probability density function values (0.01). The range of regression lines is also plotted in Fig. 2.

Data sources. In Fig. 1 we compare v_P/v_S estimates with recurrence times of slow earthquakes for five different subduction zones. These include Cascadia, Costa Rica, Mexico, southwest Japan (Nankai, Ryukyu) and Hikurangi, New Zealand. Data sources for the recurrence times are listed in Extended Data Table 2. We note that Vergnolle *et al.*[36] suggest that only the largest ETS at Guerrero recurring every four years are well documented. We also compile v_P/v_S estimates from various forms of seismic tomography models for each subduction zone (Extended Data Table 2).

31. Frederiksen, A. W., Folsom, H. & Zandt, G. Neighbourhood inversion of teleseismic *Ps* conversions for anisotropy and layer dip. *Geophys. J. Int.* **155,** 200–212 (2003).
32. Wallace, L. M. & Beavan, J. Diverse slow slip behaviour at the Hukirangi subduction margin, New Zealand. *J. Geophys. Res.* **115,** B12402 (2010).
33. Heki, K. & Kataoka, T. On the biannually repeating slow-slip events at the Ryukyu Trench, southwestern Japan. *J. Geophys. Res.* **113,** B11402 (2008).
34. Jiang, Y. *et al.* Slow slip events in Costa Rica detected by continuous GPS observations, 2002-2011. *Geochem. Geophys. Geosyst.* **13,** Q04006 (2012).
35. Obara, K. Characteristics and interactions between non-volcanic tremor and related slow earthquakes in the Nankai subduction zone, southwest Japan. *J. Geodyn.* **52,** 229–248 (2011).
36. Vergnolle, M. *et al.* Slow slip events in Mexico revised from the processing of 11 year GPS observations. *J. Geophys. Res.* **115,** B08403 (2010).
37. DeShon, H. R. *et al.* Seismogenic zone structure beneath the Nicoya Peninsula, Costa Rica, from 3D local earthquake P- and S- wave tomography. *Geophys. J. Int.* **164,** 109–124 (2006).
38. Reyners, M., Eberhart-Phillips, D., Stuart, G. & Nishimura, Y. Imaging subduction from the trench to 300 km depth beneath the central North Island, New Zealand, with Vp and Vp/Vs. *Geophys. J. Int.* **165,** 565–583 (2006).
39. Matsubara, M., Obara, K. & Kasahara, K. High Vp/Vs zone accompanying non-volcanic tremors and slow slip events beneath southwestern Japan. *Tectonophysics* **472,** 6–17 (2009).
40. Huesca-Perez, E. & Husker, A. Shallow travel-time tomography below southern Mexico. *Geofis. Int.* **51,** 281–291 (2012).
41. Ansell, J. H. & Bannister, S. C. Shallow morphology of the subducted Pacific plate along the Hikurangi margin. *Phys. Earth Planet. Inter.* **93,** 3–20 (1996).

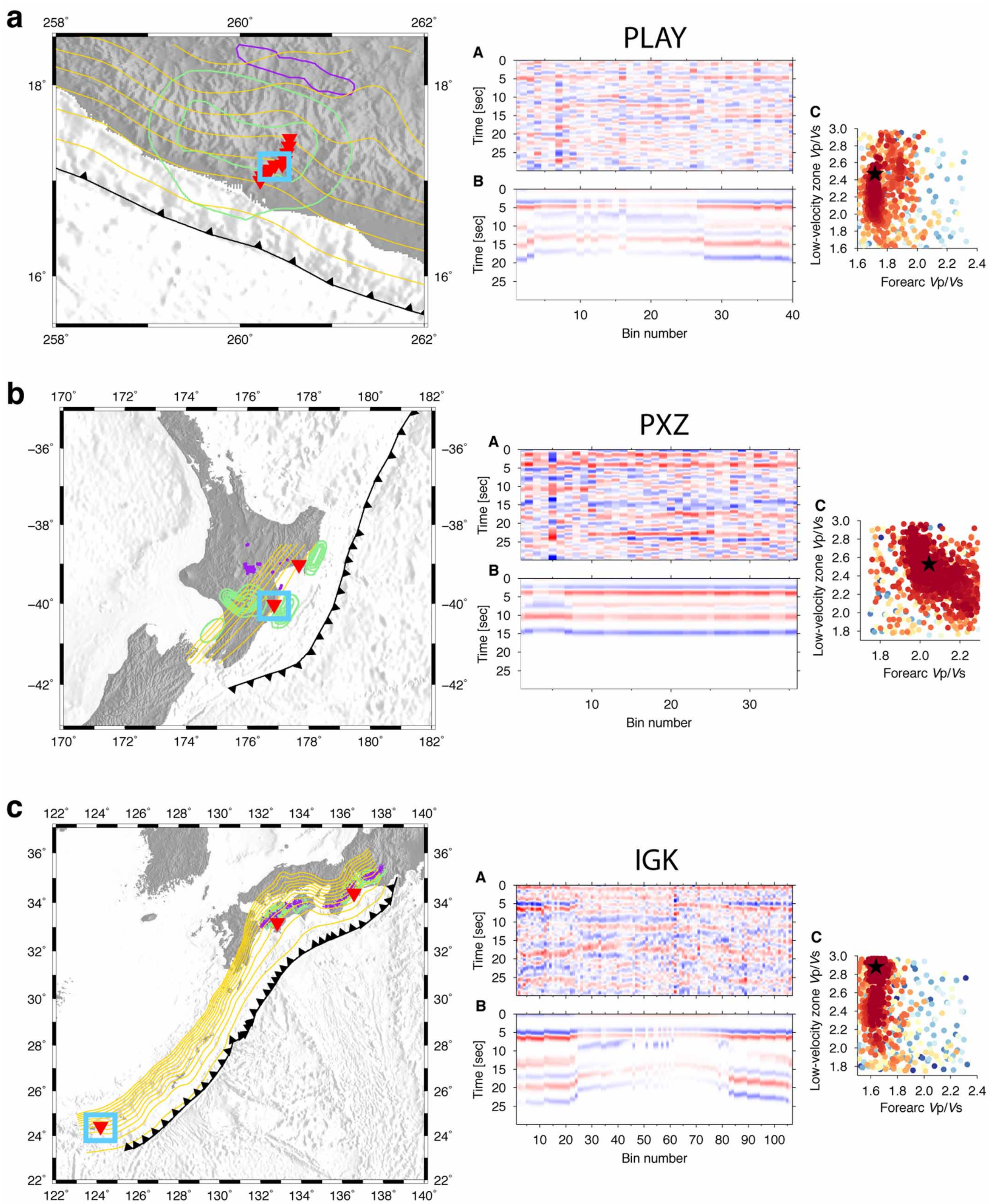

Extended Data Figure 1 | Examples of receiver functions and inversion results for each subduction zone. In **a–c** the slab contours from refs 30 and 41 are in yellow, contours of slow-slip patches from ref. 2 are in light green, contours and epicentres of tremors from ref. 2 are in purple, and station locations used in this study are shown as inverted red triangles. For a subset of stations (PLAY, PXZ and IGK, identified by the blue squares on the maps) we show the observed (top, A) and modelled (bottom, B) radial receiver functions ordered by back-azimuth and, for each back-azimuth, by slowness of the incoming P wave. **c**, A slice through model misfits, with warm colours indicating low values, showing the v_P/v_S of forearc crust versus the v_P/v_S of the low-velocity zone. The star shows the minimum value of the misfit plot (best-fitting value).

Extended Data Table 1 | v_P/v_S results from the inversion of receiver function data

	Station	Longitude	Latitude	Forearc Vp/Vs	Low-velocity zone Vp/Vs
Mexico	PLAY	-99.67	17.12	1.78 ± 0.05	2.5 ± 0.6
	XALT	-99.71	17.10	1.70 ± 0.01	2.7 ± 0.2
	XOLA	-99.62	17.16	1.69 ± 0.01	2.1 ± 0.3
	TICO	-99.54	17.17	1.66 ± 0.02	2.7 ± 0.9
	CARR	-99.51	17.21	1.71 ± 0.01	2.5 ± 0.4
	RIVI	-99.49	17.29	1.74 ± 0.01	2.8 ± 0.7
	ACAH	-99.47	17.36	1.69 ± 0.01	2.1 ± 0.8
	MAZA	-99.46	17.44	1.77 ± 0.01	2.9 ± 0.6
SW Japan	TSA	132.82	33.18	1.59 ± 0.02	2.2 ± 0.8
	WTR	136.58	34.37	1.62 ± 0.05	2.6 ± 0.2
	IGK	124.18	24.41	1.64 ± 0.01	2.8 ± 0.9
Hikurangi	PXZ	176.86	-40.03	1.98 ± 0.06	2.8 ± 0.5
	KNZ	177.67	-39.02	2.02 ± 0.03	2.5 ± 0.7

SW, Southwest.

Extended Data Table 2 | Data sources for ETS recurrence times and seismic velocity models

Subduction Zone	ETS recurrence time	Forearc crust Vp/Vs
Cascadia	Brudzinski & Allen[3]	Ramachandran & Hyndman[11]
Costa Rica	Jiang et al.[34]	DeShon et al.[37]
Central Mexico	Lowry[17]	Huesca-Perez & Husker[40]
Southwest Japan	Heki & Kataoka[33]; Obara[35]	Matsubara, Obara & Kasahara[39]
Hikurangi	Wallace & Beavan[32]	Reyners et al.[38]

Data are from refs 3, 11, 17, 32, 33, 34, 35, 37, 38, 39 and 40.